Molecular Crystals and Liquid Crystals
Publication details, including instructions for authors and subscription information:
http://www.tandfonline.com/loi/gmcl20

Hybrid Laminar Organic-Inorganic Semiconducting Nanocomposites

Z. López-Cabaña [a d], D. Navas [a d], E. Benavente [b d], M. A. Santa Ana [a d], V. Lavayen [c d] & G. González [a d]

[a] Department of Chemistry, Faculty of Sciences, Universidad de Chile, PO Box 653, Santiago, Chile

[b] Department of Chemistry, Universidad Tecnológica Metropolitana, PO Box 9845, Santiago, Chile

[c] Faculty of Chemistry, Pontifícia Universidad Católica do Rio Grande do Sul (PUCRS) Porto Alegre - RS - Brasil

[d] Center for the Development of Nanoscience and Nanotechnology, CEDENNA, Santiago, Chile

Available online: 12 Jan 2012

To cite this article: Z. López-Cabaña, D. Navas, E. Benavente, M. A. Santa Ana, V. Lavayen & G. González (2012): Hybrid Laminar Organic-Inorganic Semiconducting Nanocomposites, Molecular Crystals and Liquid Crystals, 554:1, 119-134

To link to this article: http://dx.doi.org/10.1080/15421406.2011.633852

Mol. Cryst. Liq. Cryst., Vol. 554: pp. 119–134, 2012

ISSN: 1542-1406 print/1563-5287 online
DOI: 10.1080/15421406.2011.633852

Hybrid Laminar Organic-Inorganic Semiconducting Nanocomposites

Z. LÓPEZ-CABAÑA,[1,4] D. NAVAS,[1,4] E. BENAVENTE,[2,4] M. A. SANTA ANA,[1,4] V. LAVAYEN,[3,4] AND G. GONZÁLEZ[1,4,*]

[1]Department of Chemistry, Faculty of Sciences, Universidad de Chile, PO Box 653, Santiago, Chile
[2]Department of Chemistry, Universidad Tecnológica Metropolitana, PO Box 9845, Santiago, Chile
[3]Faculty of Chemistry, Pontifícia Universidad Católica do Rio Grande do Sul (PUCRS) Porto Alegre - RS - Brasil
[4]Center for the Development of Nanoscience and Nanotechnology, CEDENNA, Santiago, Chile

Hybrid two-dimensional nanocomposites of transition metal semiconductors based on molybdenum disulfide, zinc oxide, and vanadium pentoxide, in which ultra-thin sheets of the inorganic component are stabilized by insertion into a bilayer of organic amphiphiles, are described. The resulting solids are commensurate species with characteristic stoichiometries, extremely high aspect ratio, and large organic-inorganic interfaces. Synthesis procedures and changes in the properties of the nanocomposites with respect to those of their components, depend on the structural nature of the pristine semiconductor. Derivatives of the laminar semiconductor MoS_2 are obtained by quasi-topotactic intercalation of amphiphiles into the layered inorganic matrix, being changes in the properties mainly associated to guest-host charge transfer without altering significantly the electronic structure of the sulfide. In the case of the structurally isotropic ZnO bottom-up sol-gel synthesis procedures, it is necessary to use amphiphiles as templates, producing the two dimensional confinement with significant changes in the band gap of the semiconductor. Vanadium oxide, because of bonding asymmetry, may be easily intercalated. However due to its low laying conduction band, this leads to mixed valence species. Beyond size and dimension induced bang-gap changes, the optical properties of the products, as appreciated in their absorption and emission spectra, are in general qualitatively similar to those of pristine semiconductors.

Keywords 2D hybrid semiconductors; hybrid nanocomposites; MoS_2; V_2O_5; ZnO

Introduction

Crystalline inorganic compounds of transition or post transition elements with the metal in its maximal valence-allowed oxidation state often display semiconductor behavior. Among them the inorganic semiconductors based on transition metal oxides and chalcogenides have deserved particular attention during the last decades [1]. Theoretical and experimental studies concerning the structure and the physicochemical behavior of these compounds have produced abundant fundamental knowledge as well as applications of this kind of solids,

*Address correspondence to Guillermo Gonzalez Moraga, Departament of Chemistry, Universidad de Chile, PO BOX 9845, Santiago, Chile. Tel.: 56-2-9787404; E-mail: ggonzale@.uchile.cl

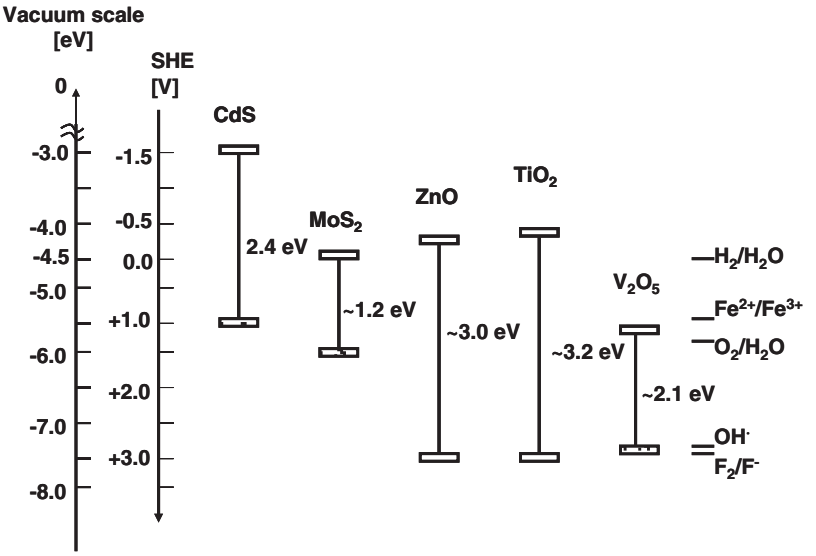

Figure 1. Absolute and relative (respect to Standard Hydrogen Electrode, SHE) energy levels of valence and conduction bands of crystalline inorganic semiconductors.

particularly in the field of catalysis [2], electrochemistry [3,4], and optics [5,6]. Nowadays the interest is strongly focused on the use of crystalline semiconductors in energy storage and in processes of conversion involved in applications in fields like photocatalysis or photovoltaics [7,8]. The semiconductor behavior of inorganic crystalline solids typically is defined by its frontier electronic structure, namely the energy of the highest full-filled valence band (VB), the energy of lowest empty conduction band (CB), and the energy difference between these bands, the band-gap (BG). The chemical reactivity of these kinds of semiconductors, particularly their redox behavior, is mainly governed by the chemical potential of both valence and conduction bands. The energy levels (absolute and relative to standard hydrogen electrode (SHE)) of frontier bands of some semiconductors in which we have been particularly interested during the last years are compared on the scheme in Fig. 1.

The most relevant processes concerning modern applications of inorganic crystalline semiconductors are shown schematically in Fig. 2. Thus, for instance, the potential of

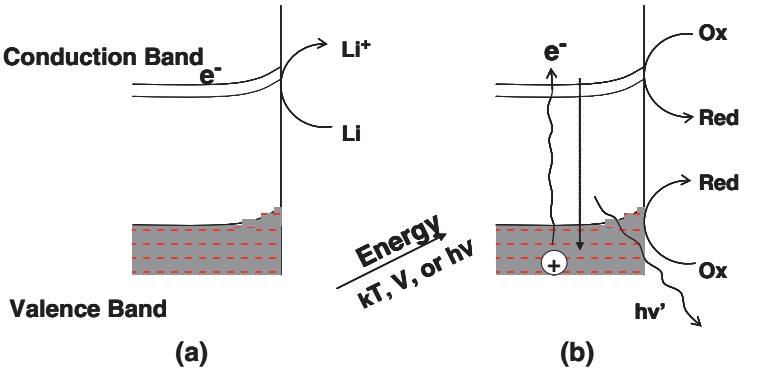

Figure 2. Physicochemical processes involved in the use of crystalline inorganic semiconductors in photocatalysis and energy conversion and storage.

a semiconductor used as positive electrode in rechargeable batteries is essentially determined by the chemical potential of the electron transferred from the electro-active metal to the semiconductor conduction band. These chemical and photochemical semiconductor-mediated phenomena are mainly heterogeneous processes. Therefore, beyond the nature of the semiconductor, the efficiency of these systems depends on the surface area available in the semiconductor for interaction. Indeed, energy conversion in such systems can be improved effectively by reducing the particles size of the semiconductor.

Graphite-like, layered inorganic solids are especially interesting because, in principle, they are always able to undergo exfoliation, leading to single laminas like graphene [9]; so they are expected to present properties different to those of their precursors. Indeed, chemical exfoliation of typical layered inorganic compounds, MoS_2, WO_3 and BN, [10] as well as a new Field Effect Transistor (FET) using MoS_2 single layers, fabricated by mechanical exfoliation, as for graphene [9], has been recently reported. It is the separation of the layers in inorganic layered semiconductors that enables changes in their properties similar to those observed for carbonaceous species. In order to contribute to answering this question we are investigating the synthesis and properties of layered organic-inorganic nanocomposites constituted, in bulk, by ultra-thin layers of the inorganic semiconductor separated each other by the organic component. This approach is centred on studying the effects of the organic component on characteristic properties of pristine semiconductor as well as on the ability of these 2-D nanocomposites to be converted, like to carbon analogues, into tubular species. In this paper we analyze comparatively the synthesis as well as main features of the chemistry of hybrid organic-inorganic two-dimensional nanostructures, based on three selected crystalline semiconductors with different atomic and electronic structures, namely MoS_2, ZnO and V_2O_5.

Experimental

Synthesis of Restacked MoS_2.

The $LixMoS_2$ ($x > 1$) was prepared by reaction of MoS_2 powder <2 mm (Aldrich) in 1.6 M hexane solution of n-butyl lithium (Merck) for 48 h under argon at 55–60°C. Dark product was centrifuged, washed with *n*-hexane, and dried under vacuum. Single layer MoS_2 was obtained from hydrolysis/exfoliation of $LiMoS_2$ in pure water in an ultrasound bath during 30 min at room temperature. Intercalation products were obtained by treating a dry *n*-hexane suspension of single layer MoS_2 with an equivalent amount of the amine. Reactions and products manipulations were carried out under argon atmosphere. Analysis:% found (calculated) for $Li_{0.1}MoS_2(C_4H_{11}N)_{0.42}$), C 10.67 (10.86), H 2.13 (2.48), N 3.94 (3.16).

Long carbon-chain amine/MoS_2 nanocomposites are prepared by addition of an aqueous solution of hexadecylamine (HDA) or octadecylamine (ODA) ($\sim 10^{-3}$ mol $\cdot$ dm^3) to the suspension of exfoliated $LixMoS_2$ (3.0×10^{-3} mol $\cdot$ dm^3), followed by stirring the reaction mixture at 60°C for 48 h. Resulting solid was centrifuged, washed with water, and dried under vacuum.

Synthesis of MoS_2 Nanotubes

The conversion of the $Li_{0.1}MoS_2(HDA)_2$ and $Li_{0.1}MoS_2(ODA)_{2.1}$ laminar species to nanotubes was achieved by hydrothermal treatment (HT) of aqueous suspensions of the nanocomposite in a Teflon-lined autoclave in a sand bath for12 h at 130°C.

Synthesis of laminar ZnO/Alkylsulphonate nanocomposite

This nanocomposite was prepared by treating the gel produced by alkaline hydrolysis of a zinc salt with the sodium sulphonate salt. Typically, an aqueous mixture of 10 mL of 1M $ZnSO_4$, 10 mL 1M Na_2CO_3, and 10 mL 1M NaOH was vigorously stirred thus leading to a white gel. Then 30 mL of a solution of hexadecylsulphonate sodium salt, $CH_3(CH_2)_{15}SO_3Na$ in water/acetone (1:1 v/v) was poured into the gel and the mixture was maintained under stirring at 60°C during 30 h. The white solid obtained was separated by centrifugation, washed with acetone/water many times and finally dried under vacuum at 80°C during 24 h.

V_2O_5/amine Laminar Intercalates: Synthesis and Conversion into Nanotubes

A mixture of *tert*-butyl alcohol and orthorhombic V_2O_5 was refluxed for 6 h to form the xerogel. Water was added to the resulting dark yellow solid and the remaining *tert*-butyl alcohol was removed together with excess water under vacuum. Water was then added to yield a suspension. The material was aged at room temperature yielding red-brown colloidal V_2O_5. The xerogel and a primary amine, dodecylamine (DDA), mixed in a molar ratio of 1:2 were stirred in ethanol for 2 h and left to age for 2 days. The mixture was then transferred into a Teflon-lined autoclave and held at 180°C for 3 days under auto-generated pressure. The product was washed with deionized water and alcohol several times and dried under vacuum.

Synthesis of the Vanadium Oxide Nano-Urchin

A solution of 10^{-3} mol of hexadecylamine (HDA) in 10 mL of pure ethanol, previously degassed by repetitive freeze-thaw cycling in argon vacuum, was mixed with $2 \cdot 10^{-3}$ mol of vanadium triisopropoxide (VOTPP). The yellow solution, obtained after vigorous stirring in an argon atmosphere for 1 h, was then hydrolyzed by adding 15 mL of doubly deionized pure water. The orange suspension obtained after stirring for 24 h was characterized by Fourier transform infrared (FTIR) and powder X-ray diffraction. The HT of the orange suspension was performed in a Teflon lined autoclave at 180°C for 7 days. From the resulting dark suspension a dark solid was separated, washed with pure ethanol and water, dried under vacuum (10^{-3} mmHg) for 48 h at room temperature, and stored under an argon atmosphere. The final VO*x* product has the composition for Analysis:% found (calculated) for $V_2O_5(HDA)_{0.83} \cdot 1.8H_2O$: C, 38.32 (39.06); H, 7.89 (8.05); N, 2.79 (2.56).

Characterization and Properties

X-ray powder diffraction analyses were performed using a SIEMENS D5000 diffractometer (Cu Kα) 1.5418 Å, operation voltage 40 kV, current 30 mA). The morphological characterization of the nanostructured products was performed by field-emission scanning electron microscopy (FESEM) using a JEOL JSM-6700F field-emission scanning electron micrograph operating at beam voltages between 1 and 10 kV. Electron transparent specimens were prepared by ion-milling techniques and placed on a holey carbon support. Transmission electron microscopy (TEM) and electron diffraction (ED) were conducted using a JEOL 2000FX operating at 200 kV. The chemical composition of the samples was determined by elemental chemical analysis using a SISONS model EA-1108 analyzer. The FTIR spectra were recorded using a KBr pellet technique on a Perkin-Elmer series 2000 apparatus in the region 4000–450 cm^{-1}. The diffuse reflectance UV–vis spectra were recorded in the

range 200 y 800 nm, at medium scan rate and slit 0.1 nm at room temperature, using a Shimadzu UV–vis spectrophotometer, 2450 PC model equipped with an integrator sphere. Barium sulfate was used in all cases as reference material. Reflectance measurements were converted to absorption spectra using the Kubelka-Munk function. The photoluminescence (PL) spectra were recorded at room temperature in solid samples using a Perkin Elmer spectrofluorometer L55.

Results and Discussion

Molybdenum Disulfide

Molybdenum disulfide has an intrinsically anisotropic layered structure, consisting of Mo-S bi-dimensional sheets which in bulk are held together by van der Waals forces [11]. There are three polytypic modifications. The 2H-MoS_2 with trigonal prismatic coordination around the molybdenum and an indirect band gap of approximately 1.2 eV [12] is the more stable one. Among the metastable polytypes the most important is 1T-MoS_2 with the molybdenum coordinated octahedrically by sulfur. This modification is an electronic conductor which becomes stable in the presence of charge excess provided, for instance, by the intercalation of electron donors in the interlaminar space. Although 2H-MoS_2 is rather inert to intercalation, it may be easily converted by reaction with strong electron donors like alkali metals [13] into the 1T modification which may be in turn intercalate topotactically with a variety of organic electron donors under rather mild conditions.

$$2H\ MoS_2 \xrightarrow{Li} 1T\ MoS_2 \qquad \text{(Ec.1)}$$

$$\underset{X=1,\Delta c=6.14\text{Å}}{Li_x\ MoS_2\ (s)} \xrightarrow{H_2O} \underset{X=0.1,\Delta c=11.4\text{Å}}{Li_x\ (H_2O)_n\ MoS_2\ (susp.)} \qquad \text{(Ec.2)}$$

$$Li_x\ (H_2O)_n\ MoS_2 \xrightarrow[Donor]{organic} \underset{x=0.01-0.3,y=0.1-2.5,\Delta c=8-50\text{Å}}{Li_x\ MoS_2\ (D)_y}$$

The X-ray diffraction patterns of the nanocomposites obtained by this way are the characteristic ones of ordered layered almost pure phases. The diffractograms are dominated by Bragg reflections at low-angle arising from crystal planes *(00l)* (Fig. 3), similar to that of the original sulfide but with interlaminar distances which are in line with the molecular dimensions of intercalated species. Products are commensurate hybrids, displaying reproducible stoichiometries as well as interlaminar distances which agree with those expected from simple molecular models.

The effect of the insertion of donor species into the interlaminar spaces of MoS_2 may be also appreciated in the change of the conductivity of the nanocomposites. As observed in Table 1, conductivity always increases upon intercalation. Such a feature is certainly associated to the change of symmetry of the coordination sphere of molybdenum. However, conductivity also depends on the nature of intercalated organic species indicating that specific guest-host charge transfer interactions is also affecting the amount of carriers in the conduction band of the inorganic component. This phenomenon may be more clearly appreciated by analyzing the co-intercalation of lithium in the nanocomposites.

The organic-intercalated MoS_2 nanocomposites described here may be intercalated with more lithium by step-wise electrochemical deposition to reach nearly one mol lithium per mol molybdenum [14]. The lithium intercalation is performed reversibly, without decomposition of the electrode, so layered 1T-MoS_2 alone or intercalated with organic donors

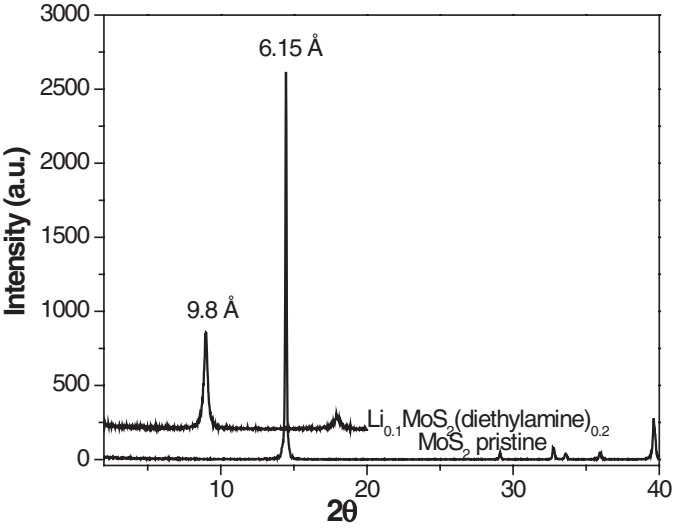

Figure 3. X-Ray diffraction patterns of nanocomposite Diethylamine/MoS_2 and pristine MoS_2.

is structurally stable towards charge accumulation. Indeed MoS_2 has been considered potentially useful as positive electrode in lithium rechargeable batteries [15]. In these devises, the potential of the MoS_2 electrode is essentially determined by electron charge transfer from lithium towards the conduction band of the sulfide, more specifically by the chemical potential of both, the electron in the layer and the lithium-ion in the interlaminar space. From such a point of view it is interesting to remark that though the band structure and the chemical potential of the electron cannot be directly modified, the potential of the electrode can be changed in some extent modulating the chemical potential of the lithium ion in the interlaminar space by selecting the organic component of the nanocomposite. This may be observed for instance in Fig. 4 where are compared the potentials of 1T-MoS_2 (restacked MoS_2) with those of the nanocomposite MoS_2/amine with different amounts of lithium. Interestingly, not only the average potential increases by the presence of the electron donor, from 1.03 to 2.72V, but are also observed notorious changes in the charge capacity as well as in shape of discharge curve. In the study of the intercalation of amines into MoS_2 it is also worth to mention the cooperative structural effects produced by the insertion of long-chain amines. Such amines are strongly amphiphilic species which under appropriate conditions self-assemble leading to different ordered structures. Among them are bi-dimensional supramolecular arrangements, mainly stabilized by inductive interactions between the hydrophobic carbon chains. In Fig. 5 is shown the diffraction

Table 1. Electronic Conductivity of nanocomposites MoS_2

Electronic Conductivity	
Compound	$\sigma(S \cdot cm^{-1})$
MoS_2	$2.10 \cdot 10^{-6}$
$Li_{0.1}MoS_2$(polyethylene oxide)$_1$	$6.60 \cdot 10^{-3}$
$Li_{0.32}MoS_2$(12-crown ether-4)$_{0.186}$	$8.50 \cdot 10^{-2}$
Li MoS_2(diethylamine)$_{0.2}$	$2.51 \cdot 10^{-1}$

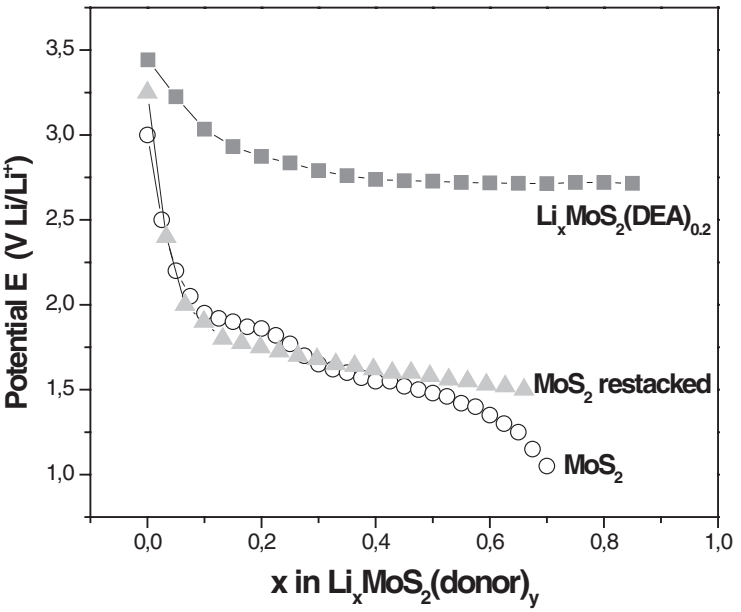

Figure 4. Quasi-equilibrium open-circuit electrode potentials (Li/Li^+) as a function of amount of co-intercalated lithium to diethylamine/MoS_2 nanocomposite and restacked MoS_2.

pattern of the product of the intercalation of hexadecylamine into MoS_2. The repeat distance in this diffractogram corresponds to the intercalation of one amine bilayer between the sulfide sheets. The solid is highly ordered, being practically monocrystalline in the direction perpendicular to the molecular plane of the laminas. Such a high ordering degree appears to be due to a cooperative effect of laminar nature of both guest and host.

The transformation of laminar species into tubular nanostructures does appear to be a rather common feature. The best example is the conversion of graphite into carbon nanotubes. Remskar et al. [16] reported the realization of MoS_2 nanotubes. The formation

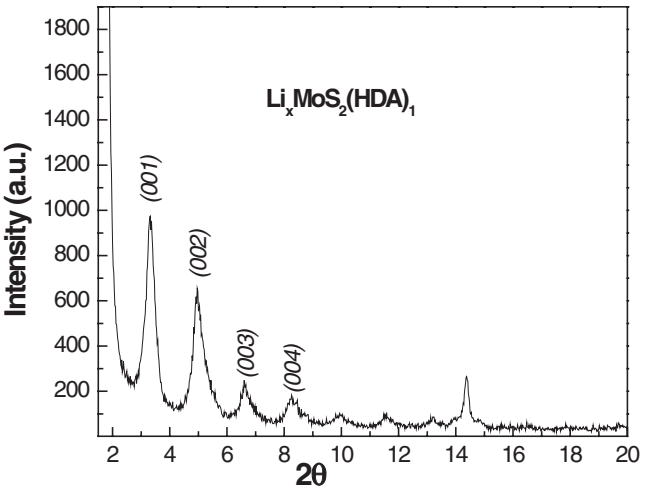

Figure 5. X-Ray diffraction pattern of the nanocomposite hexadecylamine/MoS_2.

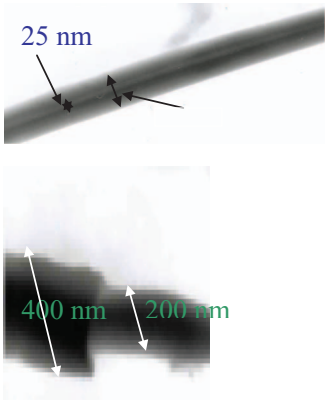

Figure 6. Transmission Electron Microscopy images of MoS_2/octadecylamine nanotubes.

of tubular structures is also observed in the chemistry of laminar semiconductor nanostructures described here. Indeed, we have also demonstrated that molybdenum/amine layered intercalates may be also converted into hybrid nanotubes [17]. In Fig. 6 is illustrated the image of a MoS_2/octadecylamine nanotubes prepared by treating an aqueous suspension of a layered precursor during 12 h at 130°C. The conversions of the lamellae of MoS_2 stabilized by long-chain amines into tubes do seem to be a rolling up process, similar to those described for graphene [9]. However, yields are by far lower than those in the case of the VOx species described below, being products morphologically always mixed.

Zinc Oxide

Obtaining layered hybrid nanostructures from semiconductors which normally have tridimensional isotropic structures is not possible by direct intercalation of organic species. This is principally because of the energy necessary for breaking ionic-covalent bonds as well as to the relatively lower thermodynamic stability of the bi-dimensional nanostructures. So the synthesis and stabilization of this kind of nanostructures require special, strategies. Bottom-up sol-gel procedures, assisted by the presence of long carbon-chain amphiphiles able to self-assembling in the form of bi-dimensional supramolecular aggregates under rather mild reaction conditions, are frequently useful for such purposes [18]. The schematic procedure shown in Fig. 7 was used for the synthesis of the layered ZnO/Alkylsulphonate

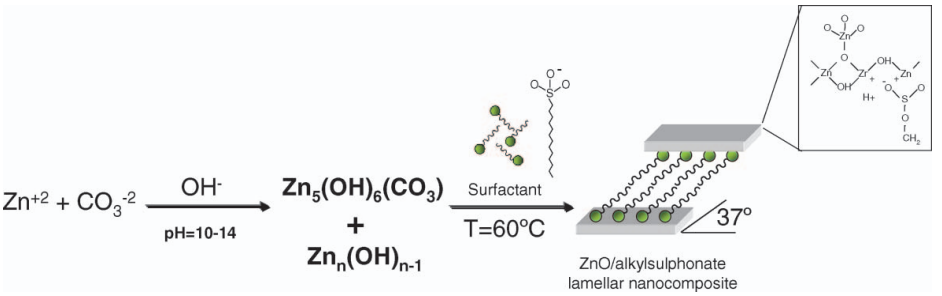

Figure 7. Representative scheme of the reactions involved in the obtainment of ZnO/alkylsulphonate lamellar nanocomposites.

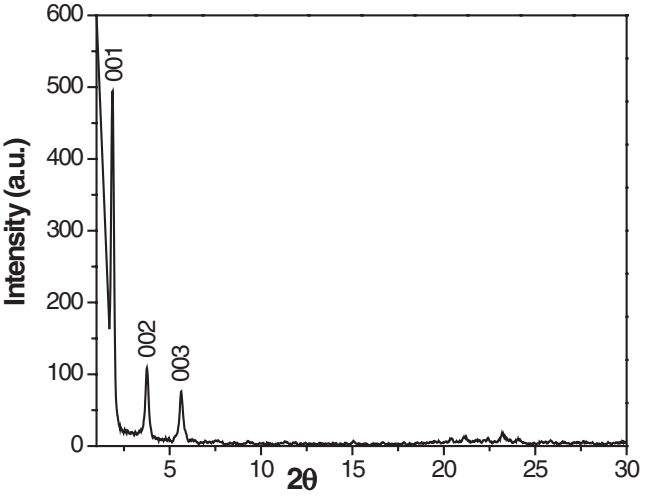

Figure 8. X-Ray diffraction pattern of ZnO/alkylsulphonate lamellar nanocomposite.

nanocomposite. In this particular case, the nanocomposite is obtained as a white precipitate from the reaction of a gel pre-formed by treating the zinc precursor, the salt $ZnSO_4$, with an alkaline mixture $NaOH/NaCO_3$ with the surfactant at 60°C. As illustrated in Fig. 8, the X-ray diffraction pattern of the sample displays Bragg reflections at a low angle corresponding to the *(00l)* crystal planes, characteristic of laminar solids, with a repeat distance of 47 Å.

In Fig. 9, the FT-IR spectrum of the product is compared with this of the free hexadecylsulphonate sodium salt. Spectra show the product contains both organic and inorganic

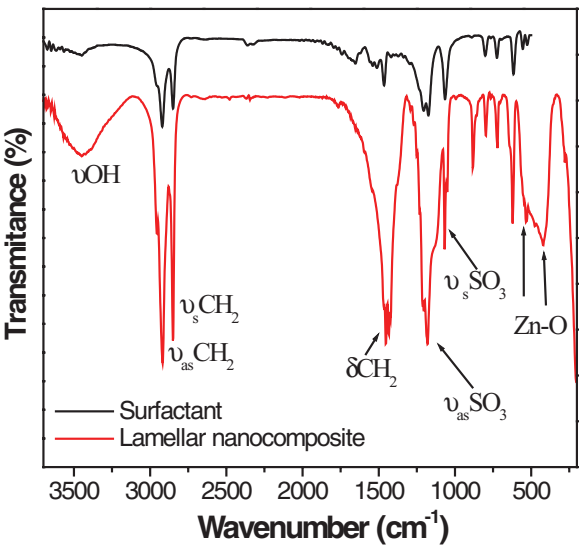

Figure 9. FTIR spectra of hexadecylsulphonate sodium salt compared with ZnO/alkylsulphonate lamellar nanocomposites.

components. Stretching vibrations of methylene group, $\nu(CH_2)_{as}$ and $\nu(CH_2)_{sym}$, are observed in both spectra centered at about 2918–2920 cm^{-1} and 2850–2851cm^{-1} respectively. The absorption bands related with the head of the surfactant, $\nu(SO_3)_{as}$ and $\nu(SO_3)_{sym}$, are observed in the product at 1180 cm^{-1} and 1069 cm^{-1} respectively. A slight shift $\nu(SO_3)_{as}$, of 6 cm^{-1} toward high energy, respect that in the free surfactant, points to an interaction of the latter with the Zn-O network. The characteristic, broad absorption band assignable to the Zn-O network is observed in the nanocomposite in the range 553–413 cm^{-1}. $Zn(OH)_2$ species also may absorb in this range; however the hydroxide also presents a characteristic strong absorption around 3400 cm^{-1}, which corresponds to the O–H stretching mode, arising from the hydroxyl groups located on the surface of $Zn(OH)_2$ particles [19]. Meanwhile the ν(OH) band observed at 3448 cm^{-1} agrees with the feature observed by the same authors in calcinated ZnO.

The composition of the product corresponds to an organic-inorganic nanocomposite with the stoichiometry $(ZnO)_1(C_{16}H_{33}SO_3)_{0.3} \cdot 0.2H_2O$ Structural information of the product may be assessed from X-ray diffraction and analytical data by considering a geometric criteria. Molecular models of surfactant molecule, built by using atomic van der Waals radii, generate a volume which is in agreement with the interlaminar distance and the stoichiometry of the product. Thus, the structure of the semiconductor in these products appears as formed by a double layer Zn-O-Zn structure of 4.8 Å thickness sandwiched between surfactant monolayers. Structurally, these products in bulk are layered solids constituted by isolated laminas of the semiconductor stabilized on each side by surfactant monolayers, which held together by van der Waals forces similarly to MoS_2/amine nanocomposites described above.

The inorganic network in the ZnO/Alkylsulphonate nanocomposite described here, constituted only by a bi-dimensional quasimolecular Zn-O sheet, cannot be identical to bulk oxide. The described product appears to be a commensurate species in which the inorganic 2-D structures are stabilized by specific interactions with the organic component forming a protective shell upon the inorganic sheet. Nevertheless, because of large organic-inorganic interfaces defined in this kind of nanocomposites, structures rich in dangling bonds and in different kind of defects may be expected. Therefore it is interesting to analyze the electronic spectra of the products. In Fig. 10 the absorption spectrum of the nanocomposite is compared with that of zinc oxide. As observed both spectra are qualitative similar, with two main broad absorption bands in the UV range. However, in the nanocomposite the band edge is noticeably shifted to higher energies. This blue shift is characteristic of the semiconductor confinement effect, arising from particle size reduction, in this case a bi-dimensional confinement.

It is worth to remark on the different chemical environments of the Zn-O network in oxide and in the nanocomposite, which in the conventional solid would correspond to chemical environment in the bulk, and in surface respectively. In spite of this, the structure of the spectra remains similar in both species. Accordingly it may be expected that photoexcitation of the layered nanocomposite does behave similarly to that of pristine semiconductor. Fig. 11 compares photoluminescence spectra of layered ZnO/Alkylsulphonate nanocomposite with that of the "bulk" ZnO. As observed, though both are rather similar, the spectrum of the nanocomposite is more strongly dominated by indirect transitions corresponding to the existence of defects and traps. Absence of the excitonic recombination band points to more efficient charge separation in the nanocomposite than in the pristine oxide. Experiments directed to test the photocatalytic ability of the nanocomposite were performed by using as model reaction the UV photodegradation of methylene blue. Results shown in Fig. 12 indicate that in the presence of the nanocomposite about 67% of the dye

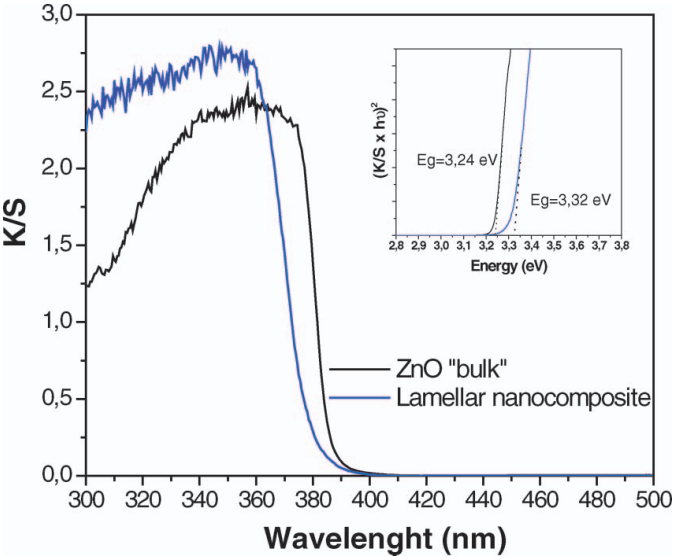

Figure 10. Reflectance diffuse spectra (after Kubelka-Mulk transformation) of "bulk" ZnO and ZnO/alkylsulphonate lamellar nanocomposite. Insert: plot $(K/S \times h\nu)^2$ against $h\nu$ showing the linear fitting to the main linear segment of the curve considering a direct band gap transition.

is degraded after 30min irradiation, while using microcrystalline ZnO as catalyst, in the same time and identical conditions, is attained a degradation of 30%.

Zinc oxide nanotubes may be prepared under hydrothermal conditions using as precursor zinc nitrate [20]. However, the hydrothermal treatment of layered zinc oxide derivatives

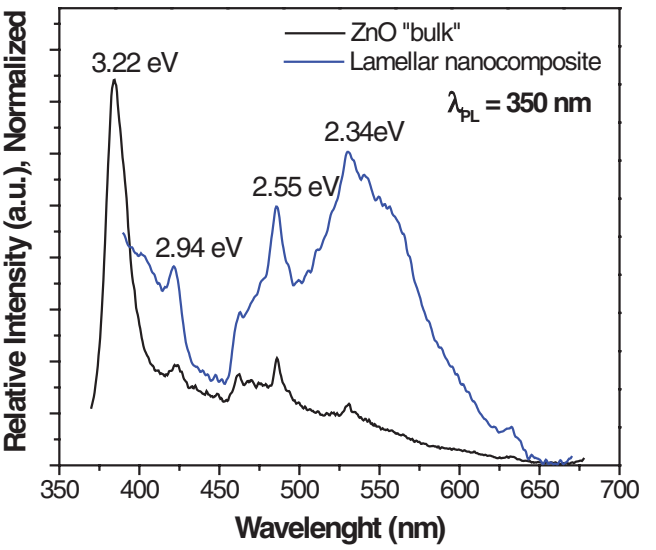

Figure 11. Photoluminescence emission spectra (λ_{PL} = 350 nm) of "bulk" ZnO compared with ZnO/alkylsulphonate lamellar nanocomposite.

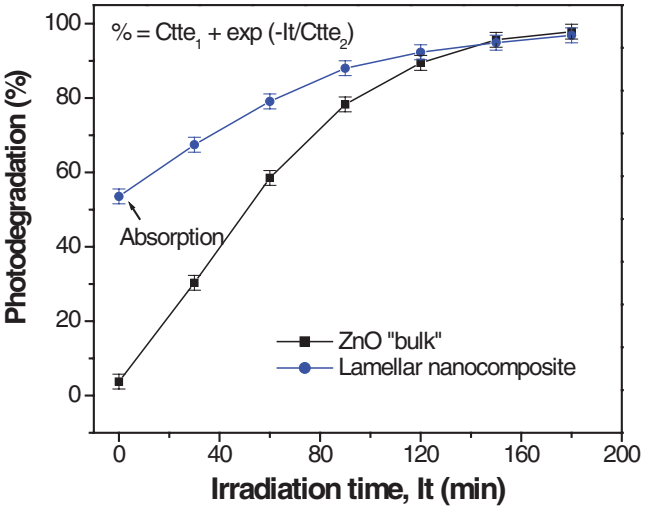

Figure 12. Photodegradation of methylene blue using ZnO "bulk" and ZnO/alkylsulphonate lamellar nanocomposite as catalysts.

like the nanocomposite described here leads to a series of nanostructures, among them nanowires and nanorods, but until now not to tubes. The interactions of the organic component with metal oxide layer and consequently the stabilization effects of the surfactant on the inorganic sheets commented above appear to be not strong enough for surviving the hydrothermal conditions. Apparently segregation of organic and inorganic components occurs, inducing the inorganic structure collapse, thus leading to tubular but bulky nanostructures. As will be discussed in next section, the conditions for obtaining tubular hybrid nanostructures are rather narrow, requiring, at least, strong interactions between organic and inorganic components.

Vanadium Pentoxide

Vanadium pentoxide has a crystal structure which is intermediate between those of MoS_2 and ZnO. Although the V_2O_5 has a tridimensional structure, in its network there is a bonding asymmetry. Indeed the crystal planes *(001)* are held together by interactions which are weaker than the V-O ionic-covalent bonds defined by the rest of crystal planes. The electronic structure of V_2O_5 is also different from those of the two semiconductors analyzed before. Although its estimated band-gap, 2.1 eV [21] is not very different from that in MoS_2, energy levels of both VB and CB are rather different in both compounds (Fig. 1). The difference with ZnO is even more marked, a notorious smaller band-gap as well as very different energies of both valence and conduction bands. The more remarkable of this oxide is the rather low energy of its conduction band characteristic which determine the physicochemical behavior and applications of this semiconductor.

Because of the low energy of its conduction band, V_2O_5 often acts as an oxidizing agent. Although xerogels, as well as amine intercalates, are prepared under mild conditions, we always observe partial reduction of the oxide, thus bearing mixed valence V(V)/V(IV) species. Redox volumetric determinations indicate that about 4% of vanadium in the samples is found as V(IV) [22]. In amine intercalates treated under somewhat more drastic

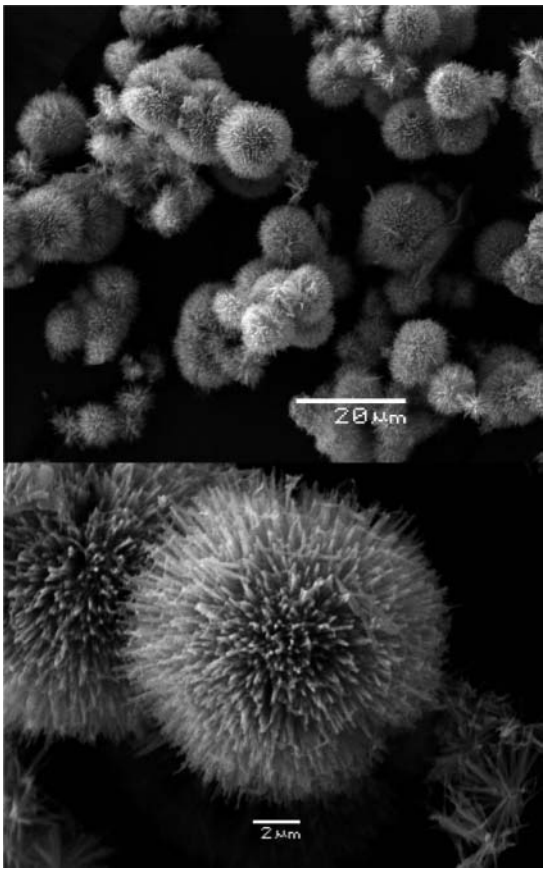

Figure 13. Scanning Electron Microscopy images of nanocomposite V_2O_5/hexadecylamine, "nanourchins".

conditions, i.e. solvothermal reactions at temperatures in the range 140–180°C during periods of times between 3 and 7 days, the relative amount of V(IV) increases reaching values between 30 and 50%. Such procedure often leads to tubular hybrid nanostructures. Indeed, this type of reactions has been widely used for producing pure phases and studying the properties of vanadium oxide nanotubes (VOx NTs) [23]. Varying the vanadium precursors and hydrothermal reaction conditions we were also able to obtain interesting three-dimensional structures like the nano-urchins (Fig. 13) [24]. Until now, only the V_2O_5/amine derivatives proved sufficiently stable to retain intercalated surfactant in the tubular products. Experiments performed using other surfactants, for instance alkylthiols, show that the organic component is segregated from the hybrid precursor at temperatures over 110°C, undergoing thereafter a complex aggregation of vanadium oxide befor finally producing pure phases of highly symmetric vanadium-oxide nanostructures in the form of "nanoflowers" or "nanocogs", Fig. 14 [25]. The mechanism for the formation of such complex nanostructures based on vanadium oxide with such good yields is still unknown. However it is believed that mixed valence state is, at least partially, responsible of rolling up processes leading to tubular structures. We think that it is still necessary to investigate the role of the surfactant in such a mechanism. Studies in such a direction are still in progress.

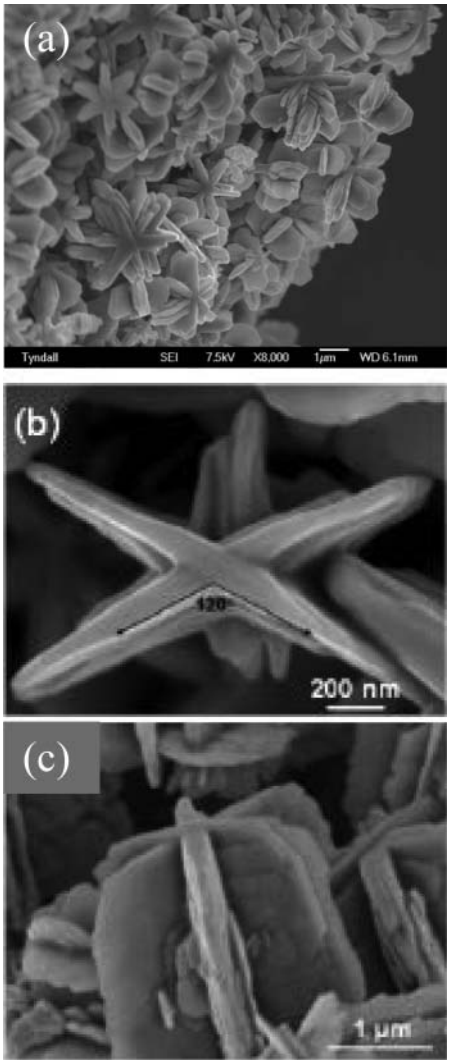

Figure 14. Scanning Electron Microscopy images of V_2O_5 nanostructures, "nanocogs" obtained from V_2O_5/thiol layered nanocomposites.

Conclusions

The synthesis of inorganic semiconductors in the form of two-dimensional ultra thin sheets stabilized by its insertion into matrices constituted by amphiphile bilayers is possible by using adequate preparation procedures, selected particularly considering standard structural habits of the inorganic precursor. Intrinsically layered semiconductors like MoS_2 or compounds with bonding anisotropic three-dimensional atomic structures like orthorhombic V_2O_5 may also lead to hybrid layered nanocomposites by quasi-topotactic intercalation processes. Meanwhile derivatives from structurally isotropic ionic-covalent structures like ZnO can not be prepared directly, but it may be obtained through bottom-up procedures

starting from oxide precursors by controlled hydrolysis using as template two-dimensional arrangements of the amphiphile.

Because structural stability towards charge excess, the effect of the intercalation of organic donors into 1T MoS_2 is essentially limited to reversible host-guest charge transfer. The ability of these nanocomposites to accumulate charge and simultaneously to enhance the activity of co-intercalate electroactive cations like Li^+, makes this kind of materials potentially useful as positive electrode for electrochemical devices.

The confinement of zinc oxide in a two-dimensional organic matrix noticeably affects the semiconductor band gap. Moreover, because of the high surface energy of the semiconductor sheet, caused by high concentration of dandling bonds and defects, inductive effects arising from the interaction with organic layer may also occurs affecting semiconductor band gap as well. That non withstanding, the photocatalytic properties of the pristine oxide are retained and even improved using the Zn/carboxylic acid layered nanocomposite.

Because of the relatively low energy of the conduction band in V_2O_5, nanochemistry this compound is dominated by redox processes leading to V(*IV*)/V(*V*) mixed valence products.

Similarly to other laminar species semiconductor nanocomposites may undergo rolling up processes generating tubular nanostructures. However yields as well as retaining the hybrid composition depends on the nature of both inorganic semiconductor and surfactants. Conversion of 2D into 1D tubular MoS_2 nanostructures is observed but mixed phases are obtained. Optimal conditions are met by vanadium pentoxide and long carbon-chain amines which produce hybrid nanotubes as well as three-dimensional arrangements of them in an almost quantitative way.

Acknowledgements

Research partially financed by FONDECYT (Contracts 1090282, 1111029) Basal Financing Program CONICYT, FB0807 (CEDENNA), Millennium Science Nucleus P10–061-F.

References

[1] Kanatzidis, M. G., & Poeppelmeier, K. R. (2007). *Prog. Solid State Chem.*, 133.
[2] Matatov-Meytal, Y. I., & Sheintuch, M. (1998). *Ind. Eng. Chem. Res.*, *37*, 309.
[3] Rao, C. N. R., Govindaraj, A., & Vivekchand, S. R. (2006). *Annu. Rep. Prog. Chem. Sect. A*, *102*, 20.
[4] Sanchez, V., Benavente, E., Santa Ana, M. A., & Gonzalez, G. (1999). *Chem. Mater.*, *11*, 2296.
[5] Ray, C. S. (2000). *J. Mater. Sci. Lett.*, *19*, 803.
[6] Li, J., & Zhang, J. Z. (2009). *Coord. Chem. Rev.*, *253*, 3015.
[7] Winter, M., Besenhard, J. O., Spahr, M. E., & Novμk, P. (1998). *Adv. Mater.*, *10*, 725.
[8] Patil, A., Patil, V., Shin, D. W., Choi, J. W., Paik, D. S., & Yoon, S. J. (2008). *Mater. Res. Bull.*, *43*, 1913.
[9] Gleim, A. K., & Novoselov, K. S. (2007) *Nature Mater.*, *6*, 183.
[10] Coleman, J. N., Lotya, M., O'Neill, A., Bergin, S. D., King, P. J., Khan, U., Young, K., Gaucher, A., De, S., Smith, R. J., Shvets, I. V., Arora, S. K., Stanton, G., Kim, H. Y., Lee, K., Kim, G. T., Duesberg, G. S., Toby Hallam, T., Boland, J. J., Wang, J. J., Donegan, F., Grunlan, J. F., Moriarty, J. C., Shmeliov, G., Rebecca, A., Perkins, R. J., Grieveson, J. M., Theuwissen, E. M., McComb, K., Nellist, D. W., & Nicolosi, P. D. (2011). *Science*, *321*, 568.
[11] Mirabal, N., Lavayen, V., Benavente, E., Santa Ana, M.A., & Gonzalez, G. (2004). *Microelectronics J.*, *35*, 37.

[12] Li, Q., Newberg, J. T., Walter, E. C., Hemminger, J. C., & Pender, R. M. (2004). *Nano Lett.*, *4*, 211.
[13] Schöllhorn, R. (1996). *Chem. Mater.*, *8*, 1747.
[14] Benavente, E., Santa Ana, M.A., Mendizabal, F., & Gonzalez, G. (2002). *Coord. Chem. Rev.*, *224*, 87.
[15] Santa Ana, M.A., Benavente, E., Páez, J., & González, G. (2000). *Bol. Soc. Chil. Quím.*, *45*, 491.
[16] Remskar, M., Mrzel, A., Skraba, Z., Jesih, A., Ceh, M., Demsÿar, J., Stadelmann, P., Levy, F., & Mihailovic, D. (2001). *Science*, *292*, 479.
[17] O'Dwyer, C., Lavayen, V., Fuenzalida, D., Newcomb, S. B., Santa Ana, M. A., Benavente, E., González, G., & Sotomayor Torres, C. M. (2007) *Phys. Stat. Sol. B*, *244*, 4157.
[18] Ruiz-Hitzky, E., Aranda, P., Darder, M., & Ogawa, M. (2011). *Chem. Soc. Rev.*, *40*, 801.
[19] Wu, D., Jiang, D.Y., Liu, J., Yuan, Y., Wu, J., Jiang, K., & Xue, D. (2010). *Nanoscale Res. Lett.*, *5*, 1779.
[20] Tong, Y., Liu, Y., Shao, C., Liu, Y., Xu, C., Zhang, J., Lu, Y., Shen, D., & Fan, X. (2006). *Phys. Chem. B*, *110*, 14714.
[21] He, Y., Wu, Y., Sheng, T., & Wu, X. (2010) *Catal. Today*, *158*, 209.
[22] Roppolo, M., Jacobs, C. B., Upreti, S., Chernova, N. A., & Whittingham, M. S. (2008). *J. Mater. Sci.*, *43*, 4742.
[23] O'Dwyer, C., Lavayen, V., Santa Ana, M. A., Benavente, E., González, G., & Sotomayor Torres, C. M. (2007). *Res. Lett. Phys. Chem.*, 32528.
[24] Lavayen, V., O'Dwyer, C., Cárdenas, G., González, G., & Sotomayor Torres, C.M. (2008). *Mater. Res. Bull.*, *43*, 3177.
[25] O'Dwyer, C., Navas, D., Lavayen, V., Benavente, E., Santa Ana, M. A., González, G., Newcomb, S. B., & Sotomayor Torres, C. M. (2006). *Chem. Mater.*, *18*, 3016.